

# Nanoscale

Accepted Manuscript



This is an *Accepted Manuscript*, which has been through the Royal Society of Chemistry peer review process and has been accepted for publication.

*Accepted Manuscripts* are published online shortly after acceptance, before technical editing, formatting and proof reading. Using this free service, authors can make their results available to the community, in citable form, before we publish the edited article. We will replace this *Accepted Manuscript* with the edited and formatted *Advance Article* as soon as it is available.

You can find more information about *Accepted Manuscripts* in the [Information for Authors](#).

Please note that technical editing may introduce minor changes to the text and/or graphics, which may alter content. The journal's standard [Terms & Conditions](#) and the [Ethical guidelines](#) still apply. In no event shall the Royal Society of Chemistry be held responsible for any errors or omissions in this *Accepted Manuscript* or any consequences arising from the use of any information it contains.

## ARTICLE

# Efficient inorganic solid solar cell composed of perovskite and PbS quantum dots†

Cite this: DOI: 10.1039/x0xx00000x

Yi Li,<sup>1,2</sup> Jun Zhu,<sup>1\*</sup> Yang Huang,<sup>1</sup> Junfeng Wei,<sup>1</sup> Feng Liu,<sup>1</sup> Zhipeng Shao,<sup>1</sup> Linhua Hu,<sup>1</sup> Shuanghong Chen,<sup>1</sup> Shangfeng Yang,<sup>2</sup> Junwang Tang,<sup>3\*</sup> Jianxi Yao,<sup>4</sup> and Songyuan Dai<sup>1,4\*</sup>

Received 00th January 2012,

Accepted 00th January 2012

DOI: 10.1039/x0xx00000x

www.rsc.org/

The lead halide perovskite solar cells have attracted great interests due to their high efficiency and simple fabrication process. However, the high efficiency heavily relies on expensive organic hole-transporting materials (OHTMs) such as 2,2',7,7'-tetrakis(N,N-dimethoxyphenylamine)-9,9'-spirobifluorene (spiro-MeOTAD), it is preferable to replace these expensive OHTMs by inorganic and low cost materials. Here, we report colloidal PbS quantum dots synthesized by a facile method and used as inorganic hole-transporting material in a hybrid perovskite solar cell. By controlling the crystalline morphology of the perovskite capping layer, the recombination process is significantly retarded. Furthermore, a pure inorganic solar cell prepared by a two-step process demonstrated a nearly 8% power conversion efficiency due to efficient charge separation by a cascade of junctions and retarding charge recombination by void-free capping layer. The stability of the inorganic solar cell was also tested with a little decay observed within ca 100 h.

## 1. Introduction

Recently, lead halide perovskite ( $\text{CH}_3\text{NH}_3\text{PbX}_3$ , X = Cl, Br, I) materials have attracted substantial attention as an excellent light absorber in thin film photovoltaic applications due to these exceptional advantages, including a large absorption coefficient, direct band gap absorption, high charge carrier mobility and long diffusion lengths.<sup>1-6</sup> In addition, it is composed of earth-abundant materials and can be prepared by low-temperature solution chemical methods.<sup>3, 7, 8</sup> Miyasaka and co-workers were the first to report  $\text{CH}_3\text{NH}_3\text{PbX}_3$  (X = Br, I)-based solar cells using liquid electrolyte in 2009 with a power conversion efficiency (PCE) of 2-4%.<sup>1</sup> In 2012, 2,2',7,7'-tetrakis(N,N-dimethoxyphenylamine)-9,9'-spirobifluorene (spiro-MeOTAD) was introduced as organic hole-transporting materials (OHTMs) for replacing problematic electrolytes and the solid state perovskite solar cell achieved an efficiency of ~ 10%.<sup>2</sup> A certified efficiency of about 20% has very recently been achieved, demonstrating the great potential of perovskite solar cells for solar energy conversion.<sup>9</sup>

Despite the remarkable achievement in perovskite solar cells, there are concerns about the cost of the frequently used OHTMs which are either small molecules, e.g. spiro-MeOTAD or conducting polymer molecules, e.g. polytriarylamine (PTAA), poly(3-hexylthiophene-2,5-diyl) (P3HT) and poly[N-9-hepta-decanyl-2,7-carbazole-alt-3,6-bis-(thiophen-5-yl)-2,5-

diocetyl-2,5-di-hydropyrrolo[3,4-]pyrrole-1,4-dione] (PCBDTPP).<sup>10-13</sup> Furthermore, these HTMs used are normally quite expensive due to complicated synthetic procedure or high-purity requirement, thus limiting these materials' large-scale application in perovskite solar cells and raising concern about the reproducibility of the solar cells. Inorganic HTMs have the advantages of better stability, ease of synthesis and low cost. Copper iodide (CuI) and copper thiocyanate (CuSCN) as effective HTMs have been applied in perovskite solar cells with the reported efficiency of 6% and 12.4%.<sup>14, 15</sup> However, manufacturing complexities for the inorganic thin films again hinder their large-scale application in perovskite solar cells.

PbS colloidal quantum dots (QDs) is one of the most intensively studied low band gap semiconductor nanocrystals owing to the high absorption coefficient, wide range of tunable band gap due to its large bohr exciton radius of 18 nm and multiple exciton generation effect.<sup>16-18</sup> By engineering the band alignment of the PbS QD layers through the use of different ligand treatments, rapid progress has been made in PbS solar cells (where PbS QDs are the only light absorber) with a certified efficiency of 8.55%.<sup>19</sup> Recently, someone also tried to using PbS QDs in perovskite solar cells. Seok and his colleagues<sup>20</sup> fabricated a  $\text{PbS}/\text{CH}_3\text{NH}_3\text{PbI}_3$  core/shell QD-sensitized heterojunction solar cells. Etgar et al.<sup>21</sup> reported co-sensitization phenomenon between  $\text{CH}_3\text{NH}_3\text{PbI}_3$  and PbS QDs in a heterojunction solar cell. However, low efficiency of less

than 4% was reported for those PbS QDs perovskite heterojunction solar cells. In this work, a two-step process was applied to prepare  $\text{CH}_3\text{NH}_3\text{PbI}_3$  layer and use PbS QDs as inorganic HTM. The influence of the crystalline morphology of the  $\text{CH}_3\text{NH}_3\text{PbI}_3$  capping layer on the recombination resistance was investigated and the solvent effect on the energy conversion efficiency was also discussed. Finally the stability of the pure inorganic solar cell was monitored.

## 2. Experimental

**2.1 Materials.** Lead (II) iodide ( $\text{PbI}_2$ , 99%), lead (II) oxide ( $\text{PbO}$ , 99%), titanium isopropoxide (97%), lithium bis(trifluoromethylsulfonyl) imide (Li-TFSI) (99.95%), 4-tert-butylpyridine (tBP, 96%), N,N-dimethylformamide (DMF, 99.9%), oleic acid (98%), 1-octadecene (90%), hydriodic acid (57 wt% in water) and hexamethyldisilathiane ( $\text{TMS}_2\text{-S}$ ) were purchased from Sigma-Aldrich. Methylamine solution (40% in Methanol) was purchased from TCI. Spiro-MeOTAD was purchased from Merck KGaA. All chemicals were used as received.

### 2.2 Synthesis.

**2.2.1 Synthesis of colloidal PbS QDs.** The synthesis of oleic acid-capped PbS QDs with a first absorption peak at 907 nm was adapted from the literatures.<sup>19, 22, 23</sup> The lead precursor was prepared by dissolving and degassing 0.45 g of  $\text{PbO}$  in a mixture of 1.5 mL of oleic acid and 18 mL of 1-octadecene at 100 °C for 5 h, until all of the reagents completely dissolved and formed a clear solution. Then the solution was cooled down to 80 °C under the argon flow and intense stirring, followed by the swift injection of the sulfur precursor formed with 215  $\mu\text{L}$  of  $\text{TMS}_2\text{-S}$  and 10 mL of 1-octadecene. The reaction mixture was additionally stirred for 30 s at 80 °C, and then the reaction mixture was cooled down to 40 °C with ice water. After synthesis, the QDs were purified and extracted. Finally, the PbS QDs were stored as a powder in the glove box.

**2.2.2 Synthesis of  $\text{CH}_3\text{NH}_3\text{I}$ .**  $\text{CH}_3\text{NH}_3\text{I}$  was synthesized according to the reported method<sup>24</sup>. A hydroiodic acid (30 mL, 57 wt% in water) was reacted with methylamine (27.86 mL, 40% in methanol) in a 250 mL round-bottom flask at 0 °C for 2 h. The precipitate was recovered by putting the solution on a rotary evaporator and carefully removing the solvent at 50 °C for 1 h. The generated yellowish powder was dissolved in ethanol, recrystallized from diethyl ether, and finally dried at 60 °C in a vacuum oven for 24 h.

**2.3 Solar cell fabrication.** Substrate preparation: Fluorine-doped tin oxide (TEC, 15  $\Omega$ /square) coated glass substrates with dimension of 2 cm  $\times$  1.5 cm were patterned by etching with Zn powder and 2 M HCl diluted in water. The etched substrates were cleaned with detergent, followed by ultrasonicated in pure water and ethanol for 30 min, and then rinsed with deionized water and ethanol, dried by air. Finally, the substrates were annealed at 500 °C for 30 min.

A dense blocking layer of  $\text{TiO}_2$  (bl- $\text{TiO}_2$ ) was spin-coated on a FTO substrate at 2000 rpm for 30 s using a mildly acidic solution of titanium isopropoxide prepared according to a reported method,<sup>25</sup> and then annealed at 500 °C for 30 min. The

mesoporous  $\text{TiO}_2$  layer was spin-coated at 5,000 rpm for 30 s onto the FTO/bl- $\text{TiO}_2$  substrate using a commercial  $\text{TiO}_2$  paste (Dyesol18NRT, Dyesol) diluted in ethanol (1:3.5, weight ratio). After drying at 50 °C, the  $\text{TiO}_2$  films were annealed at 500 °C for 30 min to remove the organic part. After cooling to room temperature, the  $\text{TiO}_2$  films were treated in a 0.04 M aqueous solution of  $\text{TiCl}_4$  at 60 °C for 1 h, rinsed with deionized water and annealed at 500 °C for 30 min.

The deposition process of perovskites on the mesoporous  $\text{TiO}_2$  films includes one-step and two-step methods. For one-step method of preparing  $\text{CH}_3\text{NH}_3\text{PbI}_3$ , a 40 wt% DMF solution of  $\text{CH}_3\text{NH}_3\text{I}$  and  $\text{PbCl}_2$  (3:1 molar ratio) was spanned on the mesoporous  $\text{TiO}_2$  films at a speed of 3000 rpm for 30 s and the perovskite was formed after heating to 100 °C for 30 minutes. For two-step method, 462 mg  $\text{PbI}_2$  was dissolved in 1 mL N,N-dimethylformamide (DMF) under stirring at 70 °C overnight, followed by filtering with 0.22  $\mu\text{m}$  pore PVDF syringe filter. The solution was kept at 70 °C during the whole procedure. 40  $\mu\text{L}$   $\text{PbI}_2$  solution was spin-coated on the mesoporous  $\text{TiO}_2$  films at 3000 rpm for 20 s, and dried at 50 °C for 3 min and 100 °C for 5 min consecutively. After cooling to room temperature, 100  $\mu\text{L}$   $\text{CH}_3\text{NH}_3\text{I}$  solution in 2-propanol (10 mg  $\text{mL}^{-1}$ ) was loaded on the  $\text{PbI}_2$ -coated  $\text{TiO}_2$  films for 20 s, which was spun at 4000 rpm for 30 s and then dried at 100 °C for 5 min.

The composition of PbS QDs HTM was 10 mg PbS QDs in 1 mL octane. The PbS QDs was deposited on the  $\text{TiO}_2/\text{CH}_3\text{NH}_3\text{PbI}_3$  film by spin coating at 3,000 rpm for 30 s. The composition of spiro-MeOTAD HTM was 72.3 mg spiro-MeOTAD, 28.8  $\mu\text{L}$  TBP, and 17.5  $\mu\text{L}$  of a solution of 520 mg  $\text{mL}^{-1}$  LiTFSI in acetonitrile in 1 mL chlorobenzene. The spiro-MeOTAD was deposited on the  $\text{TiO}_2/\text{CH}_3\text{NH}_3\text{PbI}_3$  film by spin coating at 4,000 rpm for 30 s.

Finally, 60 nm-thick Au was thermally evaporated on top of the device to form the back contact. The active area of devices were 9  $\text{mm}^2$  determined by a black mask with dimension of 3 mm  $\times$  3 mm.

**2.4 Characterization.** The surface morphology of the film was observed with a field emission scanning electron microscope (FE-SEM, sirion200, FEI Corp., Holland). The TEM images were observed with transmission electron microscopy (TEM, JEOL-2010, Japan). The UV-vis spectrum of the films was obtained using a UV-vis spectrophotometer (U-3900H, HITACHI, Japan). The current-voltage characteristics ( $J$ - $V$  curves) were measured with a Keithley model 2420 digital source meter (Keithley Instruments, Inc., OH) under the illumination of 100  $\text{mW}/\text{cm}^2$  (AM 1.5) provided by a solar simulator (solar AAA simulator, Oriel USA). The incident-photon-to-electron conversion efficiency (IPCE) measurement was conducted using a QE/IPCE measurement kit (Newport Corporation, CA). Impedance spectra were measured with an electrochemical analyzer (Autolab 320, Metrohm, Switzerland) with varying a bias potential from 0 V to 0.8 V where the potential step is 0.1 V. AC 20 mV perturbation was applied with a frequency from 1 MHz to 1 Hz. The obtained impedance spectra were fitted with ZView software (v2.8b, Scribner

Associates, USA). The Nyquist plots and the best fit results based on an equivalent circuit (Fig. 6).

### 3. Results and discussion

The oleic-acid-capped PbS QDs were synthesized according to the hot injecting method.<sup>22</sup> The first exciton absorption peak of the oleic-acid-capped PbS QDs was measured at 904 nm, which corresponds to an optical bandgap  $E_g = 1.37$  eV, as shown in Fig. 1a. Transmission electron microscopy (TEM) image (Fig. 1b) suggests that the PbS nanocrystals are highly crystalline and have an average diameter of 3.6 nm. Fig. 2a represents the band positions of the different layers in the perovskite solar cell, 2.18 which indicates that the excited electrons can vectorially transfer from PbS to  $\text{CH}_3\text{NH}_3\text{PbI}_3$  and then  $\text{TiO}_2$  and the excited holes move along the opposite direction, thus photogenerated electrons and holes are separated spatially.

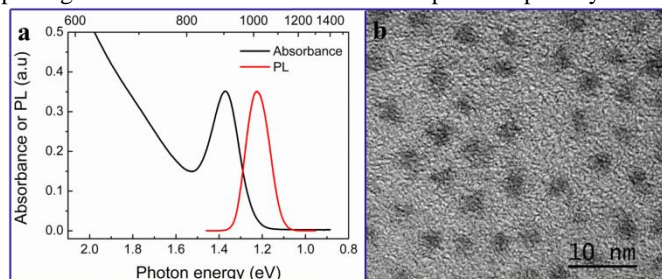


Fig. 1 Physical characterization of PbS QDs prepared by the facial hot injection method. (a) Absorption and photoluminescence spectra of PbS QDs in octane solution. (b) Transmission electron microscopy (TEM) image of oleic-acid-capped colloidal PbS QDs with exciton absorption at 904 nm. Scale bar: 10 nm.

The morphology of the deposited  $\text{CH}_3\text{NH}_3\text{PbI}_3$  has been reported to be critical for the photovoltaic performance of the perovskite solar cells. Different methods have been used for the  $\text{CH}_3\text{NH}_3\text{PbI}_3$  layer fabrication in perovskite solar cells, leading to different efficiency.<sup>26-28</sup> We fabricated the  $\text{CH}_3\text{NH}_3\text{PbI}_3$  perovskite on the mesoporous  $\text{TiO}_2$  films using traditional one-step (without using gas or toluene assisted method<sup>26, 29</sup>) and two-step methods, as shown in Fig. 2b. For one-step spin-coating procedure of preparing  $\text{CH}_3\text{NH}_3\text{PbI}_3$ , two precursors  $\text{PbCl}_2$  and  $\text{CH}_3\text{NH}_3\text{I}$  were firstly mixed in  $N,N$ -dimethylformamide (DMF) solution, and then spin-coated on the mesoporous  $\text{TiO}_2$  films. For two-step method, the mesoporous  $\text{TiO}_2$  film was firstly infiltrated with  $\text{PbI}_2$ -dissolved DMF solution by spin coating, and then a  $\text{CH}_3\text{NH}_3\text{I}$ -dissolved isopropyl alcohol (IPA) solution was spin-coated on the  $\text{TiO}_2/\text{PbI}_2$  films.

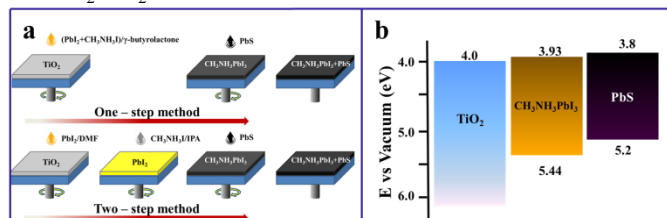


Fig. 2 (a) Energy level diagram for the corresponding materials used in our devices and (b) one-step and two-step deposition processes of perovskites on the mesoporous  $\text{TiO}_2$  nanostructure.

From Fig. 3a and b one can see that morphologies of the deposited  $\text{CH}_3\text{NH}_3\text{PbI}_3$  on the mesoporous  $\text{TiO}_2$  films are completely different due to different preparation procedures. One-step coating produces shapeless  $\text{CH}_3\text{NH}_3\text{PbI}_3$  layer on the surface of the  $\text{TiO}_2$  films (Fig. 3a), whereas the two-step method leads to the formation of  $\text{CH}_3\text{NH}_3\text{PbI}_3$  cuboids on the  $\text{TiO}_2$  films shown in Fig. 3b. Besides morphological difference,  $\text{TiO}_2$  layer is not completely covered by  $\text{CH}_3\text{NH}_3\text{PbI}_3$  using one-step method compared to full coverage with  $\text{CH}_3\text{NH}_3\text{PbI}_3$  cuboids by a two-step method, which will affect recombination of electrons in  $\text{TiO}_2$  and holes in PbS QDs as discussed later. After spinning colloidal PbS QDs octane solution, top view and cross-sectional SEM images confirm that PbS QDs have been relatively homogeneously deposited on the surface of  $\text{TiO}_2/\text{CH}_3\text{NH}_3\text{PbI}_3$  film, therefore, the void-free  $\text{CH}_3\text{NH}_3\text{PbI}_3$  cuboids capping layer would effectively inhibit the contact between PbS QDs and the bottom mesoporous  $\text{TiO}_2$  layer in the cell prepared by the two-step method. The thickness of  $\text{CH}_3\text{NH}_3\text{PbI}_3$  capping layer made by a two-step method is around 200 nm, as seen in Fig. 3f. It is apparent that the surfaces of  $\text{CH}_3\text{NH}_3\text{PbI}_3$  are smoothed by filling with the PbS QDs, resulting in a smoother plat Au film.

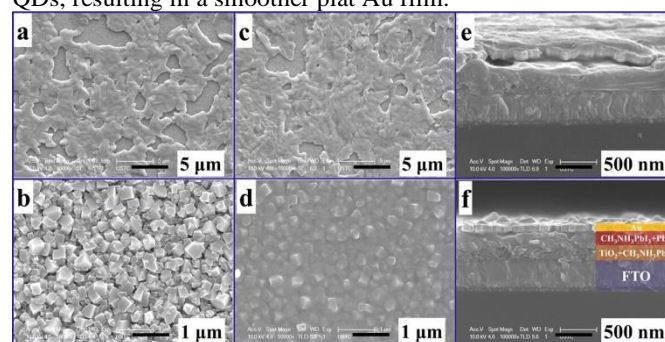


Fig. 3 Surface and cross-sectional scanning electron microscope (SEM) images of  $\text{CH}_3\text{NH}_3\text{PbI}_3$  deposited on FTO/ $\text{TiO}_2$  substrates using various deposition processes. (a)  $\text{CH}_3\text{NH}_3\text{PbI}_3$  (one-step); (b)  $\text{CH}_3\text{NH}_3\text{PbI}_3$  (two-step); (c)  $\text{CH}_3\text{NH}_3\text{PbI}_3$  (one-step) + PbS QDs (1 time); (d)  $\text{CH}_3\text{NH}_3\text{PbI}_3$  (two-step) + PbS QDs (1 time). Cross sectional SEM images of the devices for (e) one-step method and (f) two-step method. The structures of the devices are FTO/ $\text{TiO}_2$ / $\text{CH}_3\text{NH}_3\text{PbI}_3$ /PbS/Au. The mesoporous  $\text{TiO}_2$  film thickness is about 300 nm and the thickness of  $\text{CH}_3\text{NH}_3\text{PbI}_3$  capping layer made by two-step method is around 200 nm.

Because PbS QDs exhibit near-infrared absorption, some literatures have reported hybrid  $\text{CH}_3\text{NH}_3\text{PbI}_3/\text{PbS}$  solar cells with impressive  $J_{sc}$  due to the extended absorption. We investigated the optical absorption of the devices prepared herein. Fig. 4 shows the absorption spectra of the  $\text{TiO}_2/\text{CH}_3\text{NH}_3\text{PbI}_3$  and the  $\text{CH}_3\text{NH}_3\text{PbI}_3 + \text{PbS}$  QDs on  $\text{TiO}_2$  films prepared using the two-step method. The absorption of the  $\text{CH}_3\text{NH}_3\text{PbI}_3$  goes only up to 800 nm wavelength owing to its bandgap of 1.57 eV. Although the PbS QDs have an absorption in the near-infrared region as can be seen in Fig. 1a, the absorption of the  $\text{CH}_3\text{NH}_3\text{PbI}_3 + \text{PbS}$  QDs shows little contribution from PbS QDs in the near-infrared wavelength. The PbS layer's thickness is assumed to be less than 30 nm due to the low concentration PbS QDs solution (10 mg/mL) and the

fast spinning speed (3000 rpm), Compared with other literature reports<sup>20, 21, 30</sup> and this weak absorption contribution of the PbS QDs is reasonable. Likewise, little contribution of PbS QDs to the absorption is observed for the perovskite solar cell prepared by the one-step method, as seen in Fig. S1.

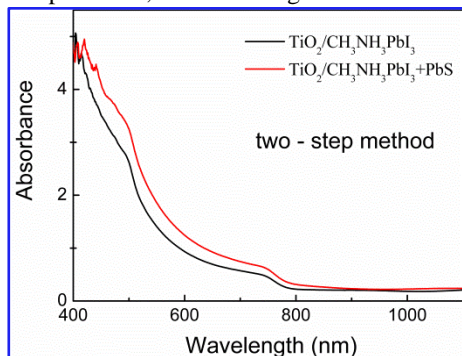


Fig. 4 UV-visible absorption spectra of  $\text{TiO}_2/\text{CH}_3\text{NH}_3\text{PbI}_3$  films before and after spinning PbS QDs. UV-visible absorption of  $\text{CH}_3\text{NH}_3\text{PbI}_3$  deposited on FTO/ $\text{TiO}_2$  substrates using two-step method with a layer of 10 mg/mL PbS QDs in octane solution. Spinning speed is 3000 rpm for 30 s.

Photovoltaic performance of the  $\text{TiO}_2/\text{CH}_3\text{NH}_3\text{PbI}_3/\text{PbS}$  solar cells based on one-step and two-step methods were evaluated. Firstly dependence of photovoltaic performance on the spin-coating number of PbS was investigated at the given PbS QD concentration of 10 mg/mL in octane and the given  $\text{TiO}_2$  thickness of 300 nm (Fig. 3e and f). Coating time for optimized solar cells was found to be 2 times for one-step method and 1 time for two-step method (Supplementary Fig. S2 and S3 and Table S1 and Table S2). In case of the device based on one-step method for  $\text{CH}_3\text{NH}_3\text{PbI}_3$  formation, PCE of  $\text{CH}_3\text{NH}_3\text{PbI}_3/\text{PbS}$  solar cells is significantly improved from 3.50% to 4.73% (35% increment) after spinning 2 times of PbS QDs, which is mainly due to increase in  $V_{oc}$  from 601 mV to 636 mV and  $J_{sc}$  from 12.49  $\text{mA}/\text{cm}^2$  to 14.17  $\text{mA}/\text{cm}^2$ . Furthermore, for the case of the device based on two-step method, PCE of  $\text{CH}_3\text{NH}_3\text{PbI}_3/\text{PbS}$  solar cells is substantially improved from 5.53% to 7.88% (43% increment) after spin-coating 1 time PbS, which is mainly due to remarkable increase in  $V_{oc}$  from 761 mV to 868 mV (14% increment) and  $J_{sc}$  from 16.78  $\text{mA}/\text{cm}^2$  to 18.69  $\text{mA}/\text{cm}^2$  (11% increment). With further increasing spin-coating number from 1 time to 4 times, no significant change in  $V_{oc}$  is observed, whereas  $J_{sc}$  is gradually decreased. One reason is further increase of the HTM thickness would increase hole transfer pathway, leading to an enhanced charge recombination but no contribution to light absorption (Supplementary Fig. S4). Another reason resulting in decreased  $J_{sc}$  is related to the influence of the octane solvent on  $\text{CH}_3\text{NH}_3\text{PbI}_3$ . The surface SEM images of the two-step method fabricated  $\text{CH}_3\text{NH}_3\text{PbI}_3$  cuboids layer before and after spin-coating the neat octane solvent are shown in Fig. S5. After spinning the octane solvent, the apparent size and shape of these cuboids are not obviously influenced. However, the photovoltaic performances of  $\text{CH}_3\text{NH}_3\text{PbI}_3$  solar cells decrease after spinning the solvent. In order to clarify the reason and comparing the new solar cell with the benchmark solar cell, we

prepared a solar cell using the widely reported spiro-MeOTAD as HTM. The reproducible PCE are shown in Fig. S6 and Table S3 is 11.11%. As can be seen in Table S3, the pretreatment of the solar cell by different solvent before coating spiro-MeOTAD HTM decreases performance of a solar cell. We used octane as solvent for PbS coating, which has a detrimental effect on the solar cell, which may be due to change of surface state of  $\text{CH}_3\text{NH}_3\text{PbI}_3$ , leading to weak interaction between  $\text{CH}_3\text{NH}_3\text{PbI}_3$  and PbS. However the detailed reason is not clear and is underway. Finally the optimized solar cells fabricated by one step and two step methods were characterized and are shown in Fig. 5a and the photovoltaic parameters are summarized in Table 1. The best solar cell was fabricated by the two step method with PbS QDs as an inorganic HTM, leading to a PCE of 7.88%. The optimized solar cell fabricated by one step method gives a PEC of 4.7%, which is similar to the very recently reported 4% achieved by a similar configuration of solar cell,<sup>20</sup> indicating our experimental condition is reliable. The nearly 70% enhancement in PCE is due to the morphology change of the  $\text{CH}_3\text{NH}_3\text{PbI}_3$  layer. The two step method as mentioned above gives a condense layer of  $\text{CH}_3\text{NH}_3\text{PbI}_3$  cuboids, which physically separate PbS HTM layer from  $\text{TiO}_2$  electron transfer layer, leading to reduction of the charge recombination. The IPCE spectra of the perovskite solar cells with PbS as HTM were measured and showed in Fig. 5b. As can be seen, there was no further extend absorption spectrum of  $\text{CH}_3\text{NH}_3\text{PbI}_3/\text{PbS}$  solar cells in the near-infrared wavelength due to the slightly amount of PbS QDs on the surface of  $\text{CH}_3\text{NH}_3\text{PbI}_3$  films, as mentioned above.

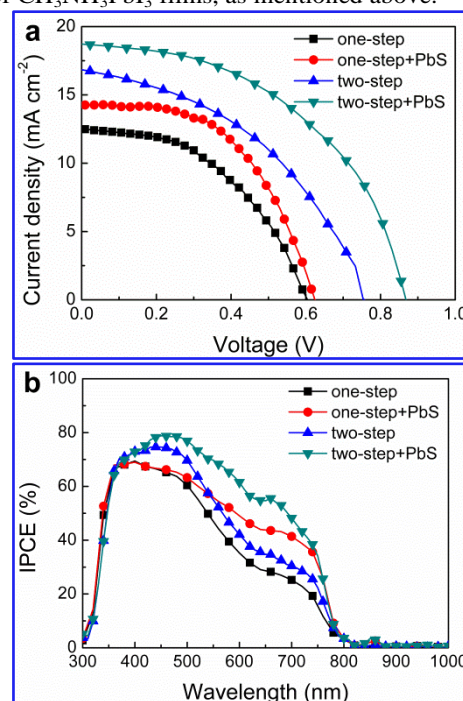


Fig. 5 Photovoltaic performance of  $\text{TiO}_2/\text{CH}_3\text{NH}_3\text{PbI}_3/\text{PbS}$  solar cells based on one-step and two-step methods before and after spinning PbS QDs. (a)  $J$ - $V$  curves and (b) IPCE spectra of  $\text{CH}_3\text{NH}_3\text{PbI}_3/\text{PbS}$  solar cells depending on the 2 layers PbS QDs for the one-step method and 1 layer for the two-step method.

Table 1 Photovoltaic parameters of TiO<sub>2</sub>/CH<sub>3</sub>NH<sub>3</sub>PbI<sub>3</sub>/PbS solar cells before and after spinning PbS QDs. The measurement was carried out under simulated one sun (100 mW/cm<sup>2</sup>).

Method	HTM	V <sub>oc</sub> (V) <sup>a</sup>	J <sub>sc</sub> (mA/cm <sup>2</sup> ) <sup>b</sup>	FF <sup>c</sup>	PCE(%) <sup>d</sup>
One-step	none	0.60	12.49	0.47	3.50
	PbS	0.64	14.17	0.52	4.73
Two-step	none	0.76	16.78	0.43	5.52
	PbS	0.87	18.69	0.49	7.88

<sup>a</sup>Open-circuit photovoltage; <sup>b</sup>Short-circuit photocurrent; <sup>c</sup>Fill factor; <sup>d</sup>Power conversion efficiency.

We employed impedance spectroscopy (IS) to investigate the factors responsible for the different voltages (636 mV vs 868 mV) in the one-step and two-step methods prepared TiO<sub>2</sub>/CH<sub>3</sub>NH<sub>3</sub>PbI<sub>3</sub>/PbS solar cells, as shown in Fig. 6. The recombination resistance ( $R_{\text{rec}}$ ) are obtained from impedance spectra where the first arc in high frequency region is related to the transport in HTM<sup>21</sup> and the second arc is related to the recombination between TiO<sub>2</sub> and HTMs.<sup>22,23</sup> The two arcs are fitted using a simplified equivalent circuit shown in Fig. 6d and the resulted  $R_{\text{rec}}$  is plotted as a function of an applied bias voltage in Fig. 6c.  $R_{\text{rec}}$  decrease exponentially for both one-step and two-step method with increasing bias voltage.  $R_{\text{rec}}$  for solar cell prepared by a one-step shows lower value than that by a two-step method as the applied bias voltage increases, which indicates that recombination in the device based on one-step method is faster compared to two-step method based devices. Thus, the solar cells prepared by a one-step method represent a lower open-circuit voltage due to higher recombination. Likewise, the two-step perovskite solar cell shows lower recombination kinetics due to its well established free-void perovskite layer to prevent the PbS QDs infiltration and thus decrease the charge recombination, leading to 230 mV higher V<sub>oc</sub> and 4.5 mA/cm<sup>2</sup> higher J<sub>sc</sub> than that by the solar cell prepared by one-step method. The stability of the best solar cell was also investigated, which is one of key factor determining the practical application of the perovskite solar cells. As seen in Table 2, the best solar cell almost remains its performance after day 2 with 8% decay compared with the fresh solar cell.

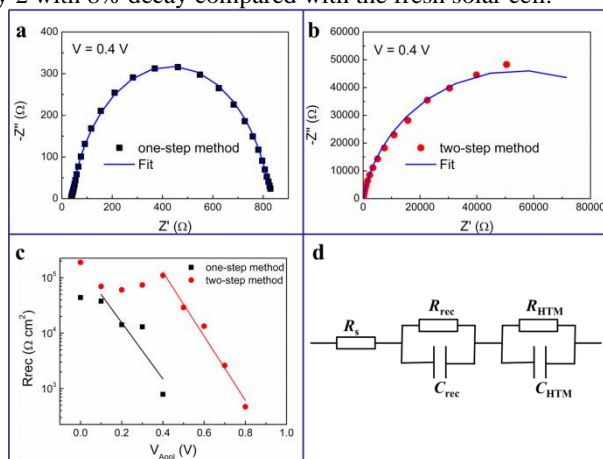


Fig. 6 Nyquist plots and recombination resistance for the perovskite solar cells with PbS as HTMs under dark condition. Representative Nyquist plots at 0.4 V biases of mesoporous TiO<sub>2</sub>/CH<sub>3</sub>NH<sub>3</sub>PbI<sub>3</sub>/PbS/Au solar cells fabricated employing (a) one-step method and (b) two-step method. (c) Comparison of recombination resistance for devices based on one-step (black) and two-step (red) deposited perovskite by applying bias voltage. (d) Equivalent circuit model employed for impedance analysis of the perovskite solar cells.

Table 2 Photovoltaic performance variation of the best CH<sub>3</sub>NH<sub>3</sub>PbI<sub>3</sub>/PbS solar cells based on two-step method under dry air at 25 °C for 4 days.

Time	V <sub>oc</sub> (V)	J <sub>sc</sub> (mA/cm <sup>2</sup> )	FF	PCE(%)
Fresh	0.87	18.69	0.49	7.88
Day 2	0.87	18.14	0.45	7.15
Day 3	0.86	18.19	0.45	7.11
Day 4	0.86	17.31	0.47	7.02

## Conclusions

In summary, colloidal PbS QDs prepared by a facile method has been successfully introduced in mesoporous perovskite solar cells as inorganic hole-transporting materials. The device based on the two-step method exhibits 70% higher power conversion efficiency than the one-step method, resulting from the denser perovskite capping layer on the surface of mesoporous TiO<sub>2</sub> films. Impedance spectroscopy suggests that compact crystalline morphology of the CH<sub>3</sub>NH<sub>3</sub>PbI<sub>3</sub> capping layer significantly retarded the recombination process between electrons in TiO<sub>2</sub> and holes in HTM. By optimized the thickness of PbS QDs, the perovskite solar cells based on PbS QDs HTM achieved a power conversion efficiency of nearly 8% with a relatively good stability. These results indicate the efficiency of PbS QDs as a low cost HTM and point out the importance of retarding recombination in a perovskite/QD hybrid solar cell.

## Acknowledgements

This work is financially supported by the National Basic Research Program of China under Grant No. 2011CBA00700, the National High Technology Research and Development Program of China under Grant No. 2011AA050527, and the National Natural Science Foundation of China under Grant No. 21403247, 21173228, 61204075, 61404142.

## Notes and references

- <sup>1</sup> Key Laboratory of Novel Thin Film Solar Cells, Institute of Applied Technology, Hefei Institutes of Physical Science, Chinese Academy of Sciences, Hefei, 230031, P. R. China.
- <sup>2</sup> Department of Materials Science and Engineering, University of Science and Technology of China, Hefei 230026, P. R. China.
- <sup>3</sup> Department of Chemical Engineering, University College London, London WC1E 7JE, UK.
- <sup>4</sup> Beijing Key Laboratory of Novel Thin Film Solar Cells, State Key Laboratory of Alternate Electrical Power System with Renewable Energy Sources, North China Electric Power University, Beijing, 102206, P. R. China.

\*Authors to whom correspondence should be addressed. Electronic mail: zhujzhu@gmail.com, junwangtang@ucl.ac.uk and sydai@ipp.ac.cn.

† Electronic Supplementary Information (ESI) available: [UV-visible absorption spectrum of perovskite based on one-step method before and after spinning PbS QDs. Photovoltaic characteristics of perovskite solar cells as a function of spin-coating number for PbS QDs]. See DOI: 10.1039/b000000x/

1. A. Kojima, K. Teshima, Y. Shirai and T. Miyasaka, *J Am. Chem. Soc.*, 2009, **131**, 6050-6051.
2. H.-S. Kim, C.-R. Lee, J.-H. Im, K.-B. Lee, T. Moehl, A. Marchioro, S.-J. Moon, R. Humphry-Baker, J.-H. Yum, J. E. Moser, M. Grätzel and N.-G. Park, *Sci. Rep.*, 2012, **2**.
3. J. M. Ball, M. M. Lee, A. Hey and H. J. Snaith, *Energy Environ. Sci.*, 2013, **6**, 1739-1743.
4. M. A. Green, A. Ho-Baillie and H. J. Snaith, *Nat. Photon.*, 2014, **8**, 506-514.
5. P. Gao, M. Grätzel and M. K. Nazeeruddin, *Energy Environ. Sci.*, 2014, **7**, 2448-2463.
6. B. Wang, X. Xiao and T. Chen, *Nanoscale*, 2014, **6**, 12287-12297.
7. K. Wojciechowski, M. Saliba, T. Leijtens, A. Abate and H. J. Snaith, *Energy Environ. Sci.*, 2014, **7**, 1142-1147.
8. D. Liu and T. L. Kelly, *Nat. Photon.*, 2014, **8**, 133-138.
9. [http://www.nrel.gov/ncpv/images/efficiency\\_chart.jpg](http://www.nrel.gov/ncpv/images/efficiency_chart.jpg), *The National Renewable Energy Laboratory (NREL)*, 2015.
10. H. Zhou, Q. Chen, G. Li, S. Luo, T.-b. Song, H.-S. Duan, Z. Hong, J. You, Y. Liu and Y. Yang, *Science*, 2014, **345**, 542-546.
11. J. H. Noh, S. H. Im, J. H. Heo, T. N. Mandal and S. I. Seok, *Nano lett.*, 2013, **13**, 1764-1769.
12. B. Cai, Y. Xing, Z. Yang, W.-H. Zhang and J. Qiu, *Energy Environ. Sci.*, 2013, **6**, 1480-1485.
13. J. H. Heo, S. H. Im, J. H. Noh, T. N. Mandal, C.-S. Lim, J. A. Chang, Y. H. Lee, H.-j. Kim, A. Sarkar, K. Nazeeruddin, M. Grätzel and S. I. Seok, *Nat. Photon.*, 2013, **7**, 486-491.
14. J. A. Christians, R. C. M. Fung and P. V. Kamat, *J Am. Chem. Soc.*, 2013.
15. P. Qin, S. Tanaka, S. Ito, N. Tetreault, K. Manabe, H. Nishino, M. K. Nazeeruddin and M. Grätzel, *Nat. Commun.*, 2014, **5**.
16. R. B. Schoolar and J. R. Dixon, *Phys. Rev.*, 1965, **137**, A667-A670.
17. G. D. Scholes and G. Rumbles, *Nat. Mater.*, 2006, **5**, 683-696.
18. J. B. Sambur, T. Novet and B. A. Parkinson, *Science*, 2010, **330**, 63-66.
19. C.-H. M. Chuang, P. R. Brown, V. Bulović and M. G. Bawendi, *Nat. Mater.*, 2014, **13**, 796-801.
20. G. Seo, J. Seo, S. Ryu, W. Yin, T. K. Ahn and S. I. Seok, *J phys. Chem. Letter.*, 2014, **5**, 2015-2020.
21. N. Mohammad K, L. Etgar, M. Grätzel, P. Gao and P. Qin, *J Mater. Chem. A*, 2014, **2**, 11586-11590.
22. M. A. Hines and G. D. Scholes, *Adv. Mater.*, 2003, **15**, 1844-1849.
23. N. Zhao, T. P. Osedach, L.-Y. Chang, S. M. Geyer, D. Wanger, M. T. Binda, A. C. Arango, M. G. Bawendi and V. Bulovic, *ACS Nano*, 2010, **4**, 3743-3752.
24. J. H. Im, C. R. Lee, J. W. Lee, S. W. Park and N. G. Park, *Nanoscale*, 2011, **3**, 4088-4093.
25. G. E. Eperon, S. D. Stranks, C. Menelaou, M. B. Johnston, L. M. Herz and H. J. Snaith, *Energy Environ. Sci.*, 2014, **7**, 982-988.
26. F. Huang, Y. Dkhissi, W. Huang, M. Xiao, I. Benesperi, S. Rubanov, Y. Zhu, X. Lin, L. Jiang, Y. Zhou, A. Gray-Weale, J. Etheridge, C. R. McNeill, R. A. Caruso, U. Bach, L. Spiccia and Y.-B. Cheng, *Nano Energy*, 2014, **10**, 10-18.
27. S. Dharani, H. A. Dewi, R. R. Prabhakar, T. Baikie, C. Shi, D. Yonghua, N. Mathews, P. P. Boix and S. G. Mhaisalkar, *Nanoscale*, 2014, **6**, 13854-13860.
28. J.-H. Im, I.-H. Jang, N. Pellet, M. Grätzel and N.-G. Park, *Nat. Nano.*, 2014, **9**, 927-932.
29. N. J. Jeon, J. H. Noh, Y. C. Kim, W. S. Yang, S. Ryu and S. I. Seok, *Nat. Mater.*, 2014, **13**, 897-903.
30. L. Hu, W. Wang, H. Liu, J. Peng, H. Cao, G. Shao, Z. Xia, W. Ma and J. Tang, *J Mater. Chem. A*, 2015, **3**, 515-518.